1993

Subparsec-Scale Radio Structure in NGC 1275--Complex Structure in the Vicinity of the Central Engine

T. Venturi

A. C. S. Readhead

Jonathan Marr
Haverford College, jmarr@haverford.edu

THE ASTROPHYSICAL JOURNAL, 411:552–564, 1993 July 10

SUBPARSEC-SCALE RADIO STRUCTURE IN NGC 1275: COMPLEX STRUCTURE IN THE VICINITY OF THE CENTRAL ENGINE

T. VENTURI[1] AND A. C. S. READHEAD
California Institute of Technology, Pasadena, CA 91125

AND

J. M. MARR[2] AND D. C. BACKER
University of California, Berkeley, CA 94720
Received 1992 July 21; accepted 1993 January 6

ABSTRACT

We present a detailed reanalysis of a series of observations of NGC 1275 at 22.23 GHz, which reveals remarkable new structures on both the scales 10^{17}–10^{18} and 10^{18}–10^{19} cm. On the scale 10^{17}–10^{18} cm a complex configuration is found in which the relative positions of the components appear to have changed by less than 10^{17} cm over the period of 1 yr covered by the observations. A persistent feature of this region is a ridge of emission extending to the north. At a distance of 1.3×10^{18} cm from the northern extreme of the source there is an abrupt change in structure accompanied by a drop of over a factor of 30 in surface brightness, and from this point there is an outflow of material at $(0.6 \pm 0.2)c$—for $H_0 = 75$ km s^{-1} Mpc^{-1}—into a limb-brightened cone of emitting material which extends 10^{19} cm to the south. Correlated bright regions on opposite sides of the cone suggest that most of the radio emission originates in a helical filament on the surface of this cone. Great care was taken in the analysis to make the best possible images from these observations, and detailed model fitting was found to be invaluable to the hybrid mapping procedure, given the complexity of the object and the limitations of the data. The dynamics of the region within 10^{18} cm of the nucleus is probably dominated by the gravitational potential of the central engine in which case these observations likely provide detailed and reliable multi-epoch models of the radio emission regions within the dynamical realm of a supermassive black hole.

Subject headings: galaxies: kinematics and dynamics — galaxies: nuclei — radio continuum: galaxies

1. INTRODUCTION

Observations of the dominant galaxy in the Perseus cluster of galaxies, NGC 1275 ($z = 0.0172$), have presented a number of intriguing problems to astrophysicists over the last half century. Seyfert (1943) drew attention to it along with five other galaxies which exhibited strong emission lines, and it is generally classified as a Seyfert 1 galaxy. However its optical morphology is unusual for a Seyfert galaxy—it is a disturbed elliptical galaxy, rather than a spiral galaxy. Its optical spectral properties are also peculiar—two emission-line systems, having velocities of $\sim$5300 and $\sim$8200 km s^{-1}, have been identified. The interpretation and significance of these two systems have been much discussed (see, e.g., Kent & Sargent 1979). The lower velocity is the systemic velocity of the galaxy, while the high-velocity system is in the foreground and moving toward NGC 1275 (Rubin et al. 1977).

There is a strong diffuse X-ray source associated with NGC 1275. The diffuse emission is almost certainly due to thermal bremsstrahlung. Coincident with the radio core, there is also a compact X-ray source (Grindlay, Branduardi, & Fabian 1980; Fabian et al. 1981; Branduardi-Raymont et al. 1981) which is very likely produced by inverse Compton scattering in the compact radio emission regions (Readhead et al. 1983a). The optical continuum is variable on a short time scale, with possible fluctuations of 1 mag in a month or so (Lyuti 1977). The nuclear region displays the usual broad and narrow emission lines of a Seyfert 1 galaxy, and CO observations reveal the presence of cold molecular gas in the inner region around the core (Mirabel, Sanders, & Kazes 1989).

The radio properties of NGC 1275 (3C 84) are extraordinary. On the scale of 10″–15″ (3.3–5.0 kpc—throughout this paper we assume an Einstein–de Sitter universe and adopt a Hubble constant $H_0 = 75$ km s^{-1} Mpc^{-1}, which yields a distance of 68 Mpc and a linear scale of 333 pc arcsec^{-1}), NGC 1275 is seen to have two oppositely directed "jets" which straddle the bright nucleus (Pedlar et al. 1986). In this respect it is similar to more distant powerful radio galaxies, which also exhibit two-sided jets. On yet larger scales of 5′–7′.5 (100–150 kpc) NGC 1275 has a large, amorphous halo (Pedlar et al. 1990), which might be an extension of the inner jetlike features. The object is very strongly dominated by a compact central component, or core. The core radio luminosity, 10^{44} ergs s^{-1}, is far greater than that of any other nearby galaxy and equals the core luminosity in the most luminous 3C galaxies, which are at redshift $z \sim 1$. These are about 30 times further away than NGC 1275, and, consequently, we can study NGC 1275 with over an order of magnitude finer linear resolution than is typically available on other galaxies with similar luminosities. The resolution available on worldwide VLBI networks at the highest frequencies makes it possible to probe NGC 1275 to within 10^{17} cm of the central engine. It is not possible to make observations with this resolution on most active galaxies with bright cores, and, of the small number of active galaxies at comparable distances. NGC 1275 has the highest core luminosity by an appreciable margin. Thus, if the basic processes responsible for the activity and high radio luminosity in NGC

[1] Present address: Istituto di Radioastronomia, via Irnerio 46, Bologna, Italy.
[2] Present address: Haverford College, Haverford, PA 19041.

1275 are similar to those in the most powerful and distant radio galaxies, this object presents the possibility of studying these processes in detail which is unmatched due to the combination of unusually high core luminosity and relative proximity. It should be noted, however, that the distant powerful radio galaxies identified in radio surveys are dominated by strong emission from their outer lobes, whereas NGC 1275 has very weak lobe emission and would have a flux density of only ~ 10 mJy at a distance corresponding to a redshift of 1. Presumably there are large numbers of such objects at $z \sim 1$.

For all these reasons, there is a strong motivation for studying NGC 1275 in the greatest detail afforded by high-frequency VLBI observations. Successful observations have been made at 90 GHz (Readhead et al. 1983b; Backer 1987; Wright et al. 1988) and at 43 GHz (Bartel et al. 1988; Krichbaum 1990; Krichbaum et al. 1992). Unfortunately, at these frequencies, the number of telescopes available, the low sensitivity, and the difficulties of calibration strongly limit the details of the strucrure which can be determined. At 22 GHz many more telescopes are available and sensitivity is far less of a problem, but calibration is still difficult and the observations even at this frequency are hardly adequate to the task of good imaging—a situation which is changing with the advent of the VLBA. Accurate 22 GHz images would greatly assist the interpretation of the 43 and 90 GHz observations, particularly if these could be attained within the same period of a few months—the time scale on which significant structural changes occur.

Since 1981 we have therefore concentrated on 22 GHz observations of NGC 1275 (Readhead et al. 1983a), and we have already published some of the results of the present observations (Marr et al. 1989; Marr, Backer, & Wright 1990). The paper by Readhead et al. (1983a) demonstrated that the object is dominated by a compact feature ~ 1.5 mas in extent to the north, which consists of a jetlike feature in p.a. $\sim -150°$ together with a feature almost orthogonal to this; a diffuse extended jet-like feature to the south; and a bright knot of emission at the southeastern end of this diffuse jet. Marr et al. (1989, 1990) showed that the knot is separating from the northern compact feature at an apparent speed of $(0.65 \pm 0.13)c$, and also drew attention to persistent features in the northern compact component, including a north-south ridge of emission, which could be associated with the orthogonal structure first detected by Readhead et al. (1983). In the present study we have reanalyzed these data in order to extract the maximum possible information from the VLBI observations. To do this, we made use of detailed and intensive model fitting before making the hybrid maps. The results justify this approach—we have been able to determine many details of the morphology of the compact northern component (thought to be coincident with the center of activity), and, in addition, some interesting new features have emerged in the jetlike southern component.

These observations and the observations of NGC 1275 at 90 and 43 GHz referenced above, together with observations at 10 GHz (Romney et al. 1982, 1984) and at 5 GHz (Unwin et al. 1982), show that the structure is complex on all scales from ~ 0.1 milliarcsec (10^{17} cm) to 13 milliarcsec (1.3×10^{19} cm). Most other powerful active galaxies which have been observed with VLBI techniques show rather simple morphologies (see, e.g., Pearson & Readhead 1988). To some degree the complexity observed in these objects is limited by the dynamic range of the images which have been made thus far, but it is clear that NGC 1275 is qualitatively different from these objects, since the structure coincident with the center of activity in NGC 1275 is complex, which is not the case in the vast majority of the objects studied thus far. This complexity may be due to the fact that we are probing much closer to the central engine in this object that in other objects and are, for the first time, studying the region in which the dynamics is dominated not by the surrounding galaxy, but by the central engine itself.

2. OBSERVATIONS AND DATA ANALYSIS

The observations were made at 22.23 GHz in three observing sessions—in 1985 February, 1985 October, and 1986 February—on a VLBI network of seven telescopes—at Effelsberg (Germany), Onsala (Sweden), Haystack (Massachusetts), Maryland Point (Maryland), Green Bank (West Virginia), the VLA (New Mexico), and the Owens Valley (California). The data for all the observations were recorded using the Mark II recording system with a bandwidth of 2 MHz and were correlated with the JPL/Caltech Block-2 Correlator in Pasadena and analyzed using the Caltech VLBI software package (Pearson 1991). Details of the observations are given in Marr et al. (1989).

2.1. *Modeling and Mapping*

It has been a hope ever since hybrid mapping was first developed (Wilkinson et al. 1977; Readhead & Wilkinson 1978; Readhead et al. 1980) that an atuomatic method of making maps from the phase-corrupted visibility data obtained in VLBI would be devised. Much progress has been made in this area (see, e.g., Pearson & Readhead 1984; Readhead 1990), but the process is still far from automatic. VLBI imaging requires a lot more care and judgment than does imaging from coherently phased arrays such as the VLA. In the case of NGC 1275 the structure is complex, and VLBI images of this object, especially those at high frequencies, must be interpreted with caution.

Model fitting accomplishes two purposes—first it is a powerful tool for refining the calibration of the observations—and second it makes an approximation of the structure in terms of a small number of free parameters. When used properly, model fitting can give important feedback on which sections of the data can be trusted, and which are suspect. In addition, model fitting makes it possible to probe structures which are somewhat smaller than the beamwidth of the instrument. This is an example of *superresolution*, and it should be treated with caution. It has been found in numerous cases that the sizes and positions of components can be inferred down to about a factor 2 smaller than the instrumental beamwidth by means of model fitting (e.g., Zensus, Hough, & Porcas 1987).

A major difference between this analysis and our previous maps at comparable resolution is that by starting with a model which fits the data extremely well we are able to make a more reliable—higher dynamic range—hybrid map. The process of model fitting and hybrid mapping with VLBI data is basically a process of defining the best filter for the data. The best results are obtained if one starts with a very good model and limits the number of hybrid mapping steps to a minimum. The reason for this is that hybrid mapping with full self-calibration has a very large number of degrees of freedom. It is all too easy with hybrid mapping to fit significant features in the visibilities by noise which is spread out across the map, and hence to end up in a minimum which is quite far from the global minimum and yet have good agreement between the map and the data. Model fitting is much more exacting, since there are few degrees of freedom in comparison with a hybrid map even for

models with a dozen or so components such as we use here. Model, fitting, by forcing the components to be simple and to have positive brightness, finds a simple solution which fits the data fairly well. If this model is then used as the starting point for hybrid mapping, the mapping step starts off close to the global minimum, and it can refine the model significantly without introducing spurious structures. In the present case, because of the complexity of the object, the paucity of the data, and the limitations of calibration at high frequencies, intensive model fitting is advisable, and the quality of the final map is strongly influenced by the quality of the starting model.

2.2. *The First Epoch*

We decided to begin with the data from the epoch of 1985 February because this was the best available data set in terms of both data quality and quantity. As a starting point, we began with the five-component model that we had derived in fitting our 1981 observations (Readhead et al. 1983a), that is, a northern structure formed by a core and a two-component jet, and extended southern component containing $\sim 35\%$ of the total flux density, and a pointlike component located at the southern edge of this extended emission. It was immediately clear that the object had changed significantly and that the 1981 model was far too simple to be used as a starting model. We therefore examined the 1985 visibilities and tried to pick out features in the amplitudes which occurred on a small number of closely spaced baselines. We found that it was possible to fit simple two- or three-component models to the longest baselines, but that there was very little agreement between these models from baseline to baseline, indicating that the structure was very complex. We proceeded by combining the models derived for separate baselines and by a process of trial and error, and eventually we managed to obtain reasonable fits to the data on four baselines from Europe to the US east coast with four- and five-component models. In extending these models to more baselines we found that no progress could be made without including more components, and our final model comprised a total of 13 components.

We reached several local minima in the multidimensional space during the interactive modeling, and while the agreement factors were still poor (>3) we sometimes found two or three models with comparable agreement factors and significantly different structures. The agreement factor is effectively the reduced χ^2, or χ^2_ν. Careful inspection of the fit of the model to the visibility amplitudes and closure phases was necessary to discriminate between these models, and we sometimes had to proceed with two different models in parallel until one could be pushed to significantly better agreement factors than the other.

As we proceeded we found that the chief difficulty in this procedure was that of obtaining any model at all with agreement factors less than three. It was not the case that many different models gave fits as good as this. At times when the model fitting program had reached a local, but clearly not global, minimum, progress could only be made by fitting to the amplitudes and then the closure phases alternately, or, sometimes, by adjusting the relative noise levels. Not until we had reached agreement factors on both the amplitudes and the closure phases of less than three did we feel that we had pushed the model into the vicinity of the global minimum, and that the major features of the model were correct.

Our final 13-component model (see Table 1) for the 1985 February epoch gives an agreement factor of 2.7 for the visibility amplitudes and 2.6 for the closure phases, and it reproduces many of the finest details in the visibility plot, as shown in Figure 1*a* and 1*b*.

2.3. *The Second and Third Epochs*

A comparison of the visibilities from the three epochs showed that significant changes in structure had occurred in NGC 1275 over the course of the year. We started with the model derived for the first epoch, and found that it was very easy to obtain good fits to the other two epochs, with a comparatively small number of iterations. This gave us confidence that our model for the first epoch was basically correct, since there were significant differences in the (u, v) coverage obtained in observations at the three different epochs. The ease with

TABLE 1

1985 FEBRUARY MODEL AND PHYSICAL PARAMETERS

	1985.17 MODEL				PHYSICAL PARAMETERS				
COMPONENT	S (Jy)	r (mas)	θ	ϕ (mas)	T_b (K)	B_{eq} (G)	Pressure (dyne cm^{-2})	U_{min} (ergs)	t_{synch} (yr)
A	1.78	0.00	0°	0.25	10^{10}	0.6	0.025	4×10^{50}	0.5
B	1.90	0.40	−140	0.21	1.5×10^{11}	0.7	0.03	4×10^{50}	0.4
C	5.45	0.71	−135	0.43	10^{10}	0.5	0.015	1.7×10^{51}	0.7
D	2.41	0.49	−80	0.31	10^{11}	0.5	0.02	7×10^{50}	0.6
E	1.60	0.58	−116	0.34	5×10^{10}	0.4	0.013	6×10^{50}	0.85
	0.70	1.55	−151	0.44	1.2×10^{10}	0.3	0.005	5×10^{50}	1.7
	0.98	1.56	−162	0.21	7×10^{10}	0.6	0.02	3×10^{50}	0.6
	2.98	2.09	179	1.52	4×10^{9}	0.15	0.0015	6×10^{51}	4
	4.91	4.62	−179	1.94	4×10^{9}	0.13	0.0012	10^{52}	5
	1.62	6.40	177	1.49	2.5×10^{9}	0.12	0.001	4×10^{51}	6
	3.25	9.70	171	1.14	8×10^{9}	0.2	0.002	4×10^{51}	3
K	0.34	10.22	173	0.31	1.2×10^{10}	0.3	0.006	2×10^{50}	1.5
	10.11	10.49	−178	2.94	4×10^{9}	0.12	0.001	3×10^{52}	6

NOTES.—Parameters of the model derived from model fitting to the 1985 February observations. Components identified in the text and marked on Fig. 2 are given in col. (1); col. (2): flux density (in Jy); col. (3): distance from component A (in mas); col. (4): position angle of component relative to component A; col. (5): the geometrical mean of the major and minor axes (FWHM) of the component in milliarcsec; col. (6): the brightness temperature at 22.23 GHz; col. (7): the equipartition magnetic field in G; col. (8): the total pressure, due to particles plus magnetic field assuming equipartition, in dynes cm^{-2}; col. (9): the minimum energy of the component in ergs; col. (10): the time in yr in which electrons radiating predominantly at 22 GHz will lose half their energy.

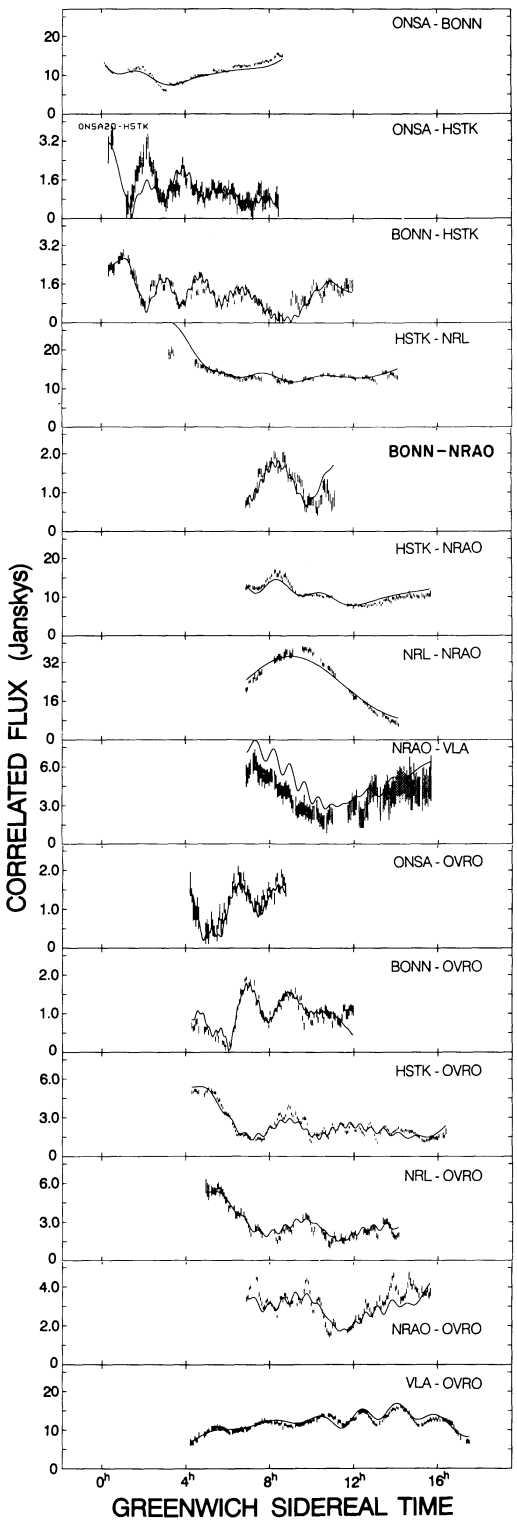

FIG. 1*a*

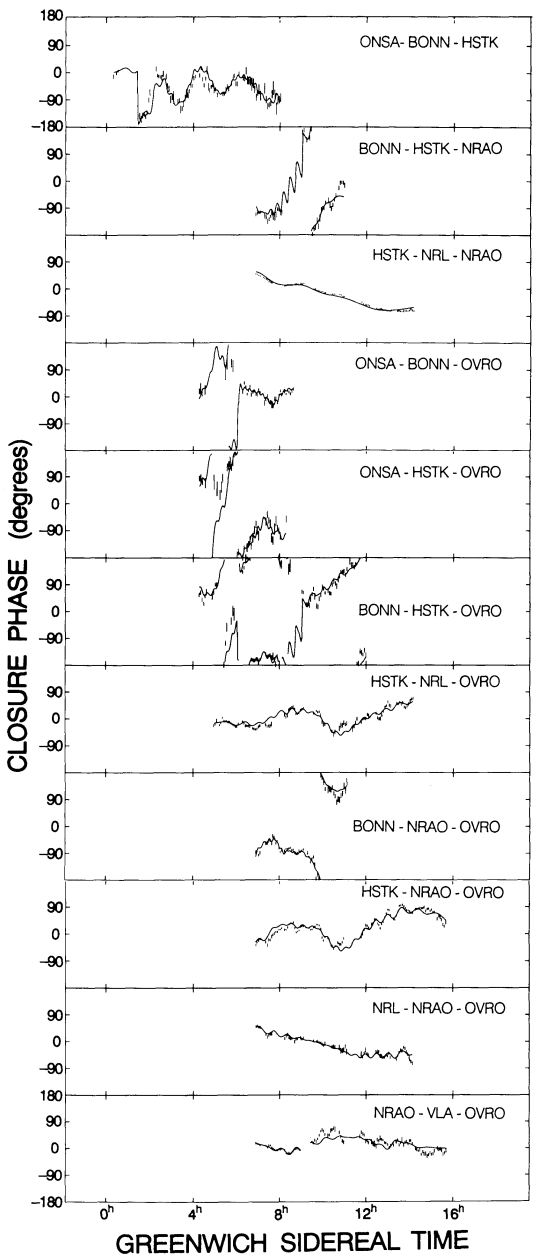

FIG. 1*b*

FIG. 1.—First epoch (1985.17) visibilities of NGC 1275: (*a*) amplitudes before self-calibration, and (*b*) closure phases. The solid curves show the fits to the data of the 13-component Gaussian model given in Table 1. Note that this model is able to reproduce many of the fine details of the visibilities on all baselines and triangles.

TABLE 2

1985 OCTOBER and 1986 FEBRUARY MODELS

	1985.83				1986.17			
COMPONENT	S (Jy)	r (mas)	θ	ϕ (mas)	S (Jy)	r (m)as)	θ	ϕ (mas)
A	1.62	0.00	0°	0.24	1.27	0.05	−14°	0.37
B	1.92	0.39	−139	0.25	1.67	0.43	−147	0.36
C	5.59	0.73	−141	0.47	7.20	0.74	−144	0.52
D	2.50	0.46	−84	0.44	2.80	0.39	−95	0.42
E	1.76	0.60	−111	0.35	0.63	0.60	−105	0.42
	0.49	1.29	−134	0.41	0.33	1.26	−133	0.16
	0.51	1.89	−168	0.30	0.14	2.08	−172	0.04
	4.05	1.98	−171	1.57	2.52	1.63	−171	1.15
	2.61	4.42	−174	1.29	5.87	3.76	−172	2.80
	6.65	9.73	172	1.97	11.11	10.05	173	2.31
K	0.76	10.51	174	0.35	0.50	10.80	174	0.55
	11.45	10.50	−175	2.83	6.10	10.96	−176	1.99

NOTES.—Parameters of the models derived from model fitting to the 1985 October and 1986 February observations. The columns are the same as the first four in Table 1, except that in the 1986 February model the position has been shifted to minimize the relative changes in position in components A–E.

which we could fit the two later epochs, and the similarities between the three models lend considerable credibility to the reliability of our first model, since it was able correctly to predict the visibilities in regions of the (u, v) plane that were not sampled in the first epoch. We regard this as a reassuring indication of the reliability of our models.

The agreement factors obtained are 1.7 and 1.9 (amplitude and closure phases respectively) for the 1985 October observations, and 2.2 and 2.7 (amplitude and closure phases respectively) for the 1986 February observations (see Table 2). The models corresponding to the three epochs are shown in Figures 2*a*–2*c*, where the Gaussian components of each model have been convolved with a circular beam with half-power beamwidth = 0.1 mas. The details of the northern feature can be seen more clearly in Figures 3*a*–3*c*.

At the close of the model fitting stage we had obtained three recalibrated data sets in which we had great confidence—we believe that there are no calibration errors greater than 5% in the amplitudes and 2° in the closure phases remaining in these corrected data sets. This is a low level of calibration error for observations at 22 GHz because our iterative procedure of model fitting and recalibration has significantly reduced the level of errors obtained in the original calibration.

It is clear from the models that the northern feature consists of a number of very compact components extending along a line at position angle −135° → −150° (components "A," "B," and "C"), plus an extension to the north of this group (components "D" and "E"). In our previous analysis (Marr et al. 1990) we found clear evidence for this northern extension, or ridge, but the exact disposition of subcomponents was unclear.

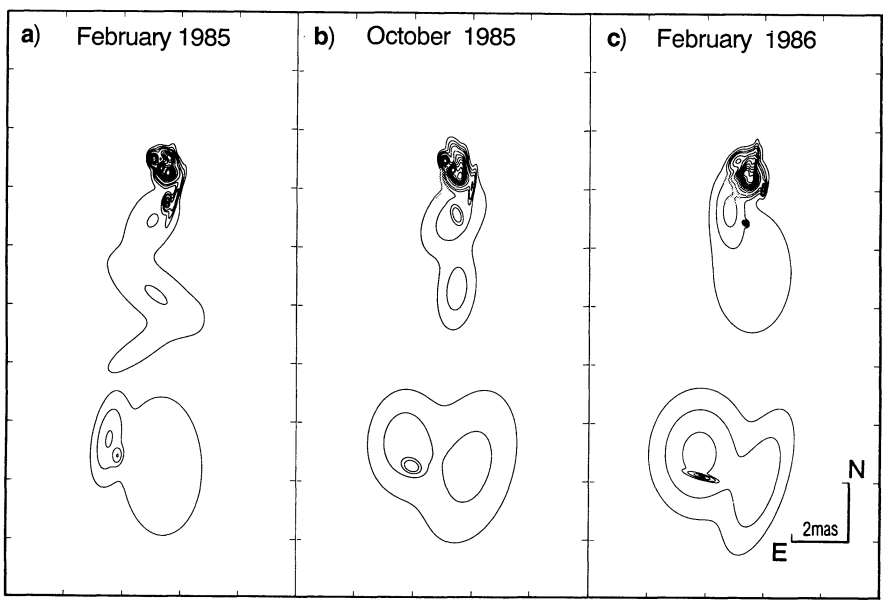

FIG. 2.—Models derived from the model fitting for the three epochs: (*a*) 1985.17, (*b*) 1985.83, and (*c*) 1986.17. The Gaussian components have been convolved with a circular beam of 0.1 mas. The contour levels are 1%, 3%, 6%, 10%, 20%, 30%, 40%, 50%, 60%, 70%, 80%, 90% of the peak brightness levels of 0.4 Jy beam^{-1}, 0.35 Jy beam^{-1}, and 0.29 Jy beam^{-1}, respectively. The plot scale is 2.0 milliarcsec per interval.

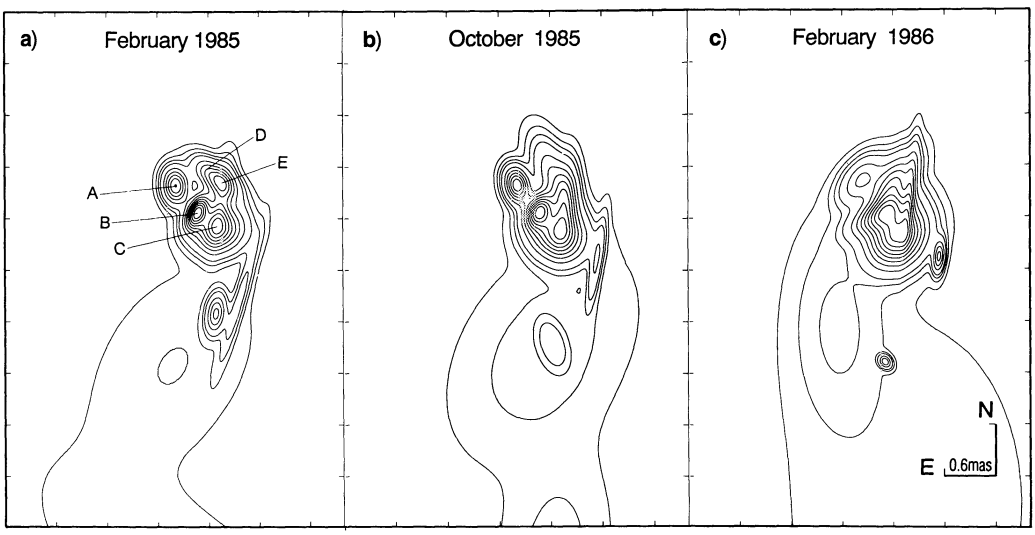

FIG. 3.—Detailed view of the model components in the northern region: (*a*) 1985.17, (*b*) 1985.83, and (*c*) 1986.17. The restoring beam, contour levels, and peak brightnesses are the same as in Fig. 2. The plot scale is 0.6 milliarcsec per interval.

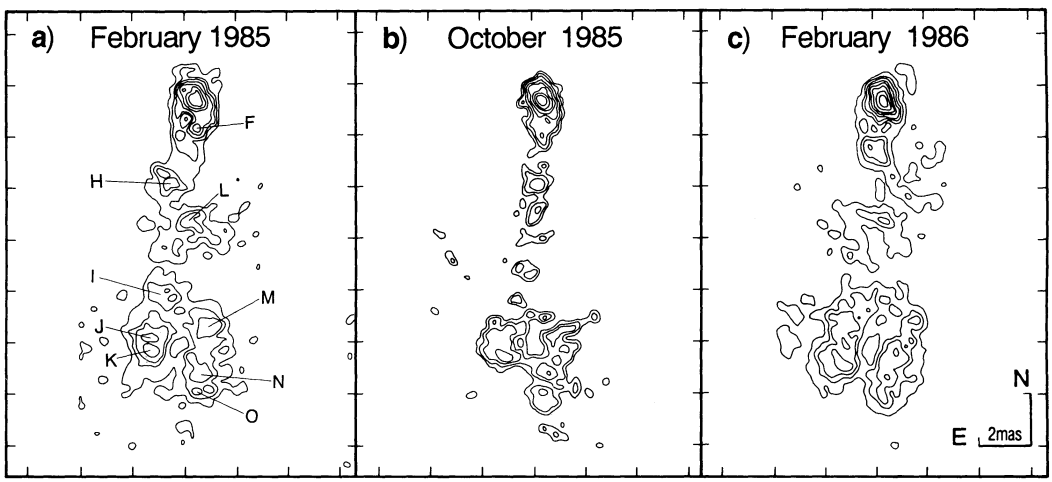

FIG. 4.—The final hybrid maps for the three epochs: (*a*) 1985.17, (*b*) 1985.83, and (*c*) 1986.17. The delta functions plus noise have been convolved with a circular Gaussian beam of 0.3 milliarcsec (FWHM). The contour levels are (*a*) −1%, 1%, 3%, 5%, 10%, 20%, 30%, 50%, 70% peak; (*b*) −2%, 2%, 3%, 5%, 10%, 20%, 30%, 50%, 70% peak; and (*c*) −1%, 1%, 3%, 5%, 10%, 20%, 30%, 50%, 70% peak. The plot scale is 2.0 milliarcsec per interval.

Model fitting has enabled us to determine the structure in far more detail than was possible with hybrid mapping starting with a simple model.

The next step in our data reduction was to make hybrid maps for each epoch, using the corresponding model derived from the model fitting as the first input model. Convergence between the visibilities and the models was reached after only two cycles of self-calibration, Fourier inversion, and "CLEANing." The maps are shown in Figures 4*a*–4*c*. These maps have been "restored" by convolution with a "CLEAN" circular Gaussian beam having a half-power beamwidth of 0.3 mas. Contour levels are given as percentages of the peak flux. If we define the dynamic range as the ratio of the peak flux density level per beam to the rms noise level in an empty region of sky, we have achieved a dynamic range greater than 300:1 in all three maps, as shown in Table 3, however, there remain some spurious features caused by residual small calibration problems, which have not been eliminated in the model fitting, and the sparse (*u*, *v*) coverage, which lead us to trust these maps only down to the ~1% contour. The hybrid map of the 1985 February observations is particularly good since this is the best of the three data sets. The fits to the self-calibrated data of the delta functions comprising the first epoch hybrid map are shown in Figure 5. Comparison with Figure 1 shows that hybrid mapping has succeeded in fitting the data considerably

TABLE 3

DYNAMIC RANGE AND FLUX DENSITIES ON THE HYBRID MAPS

Epoch	rms (mJy/*b*)	Dynamic Range	Total Flux (Jy)	Core Flux (Jy)	Flux K (Jy)
1985.17.....	5.0	440	32.5	15.2	1.4
1985.83.....	8.2	305	29.1	14.6	1.6
1986.17.....	4.8	505	34.0	16.4	2.0

NOTES.—Parameters of the map for each epoch of observation. Col. (1): epoch; col. (2): noise in the map; col (3): dynamic range, defined as the ratio between the peak in the map and the rms in a region of blank sky; col. (4): total flux density in the map in Jy; col. (5): flux in the northern component (see Fig. 3*a*–3*c*) in Jy; col. (6): flux density of the subluminal knot K in Jy, as measured on the hybrid maps.

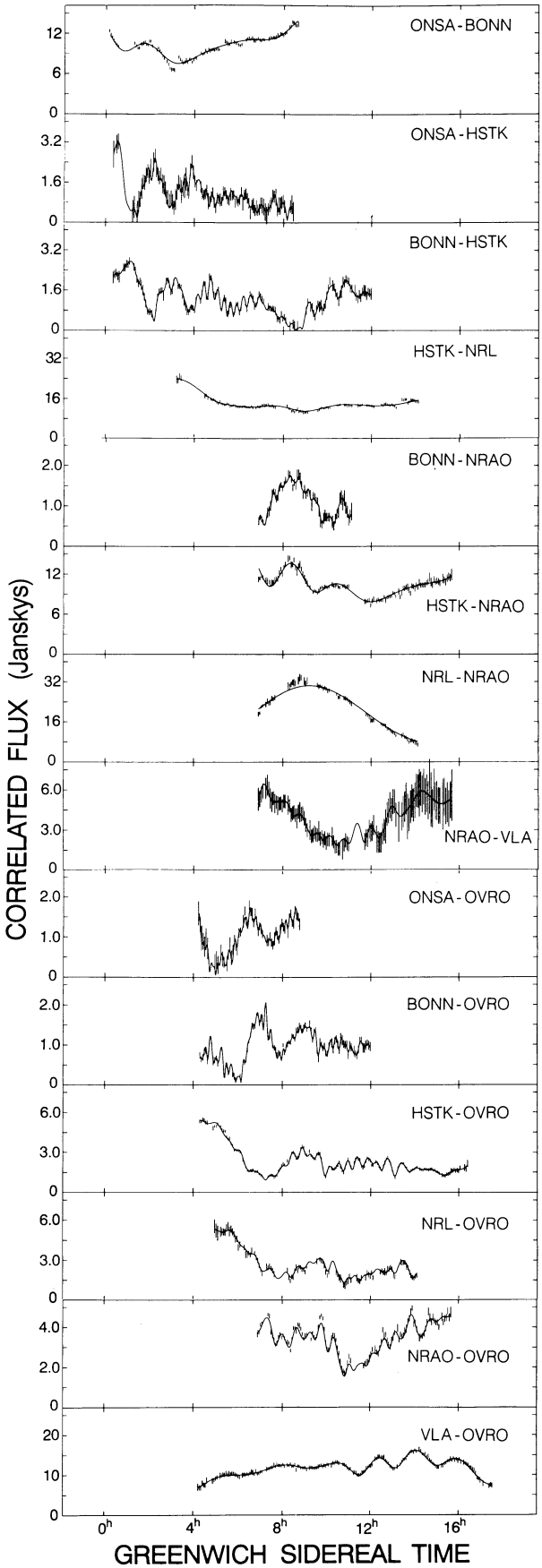

FIG. 5a

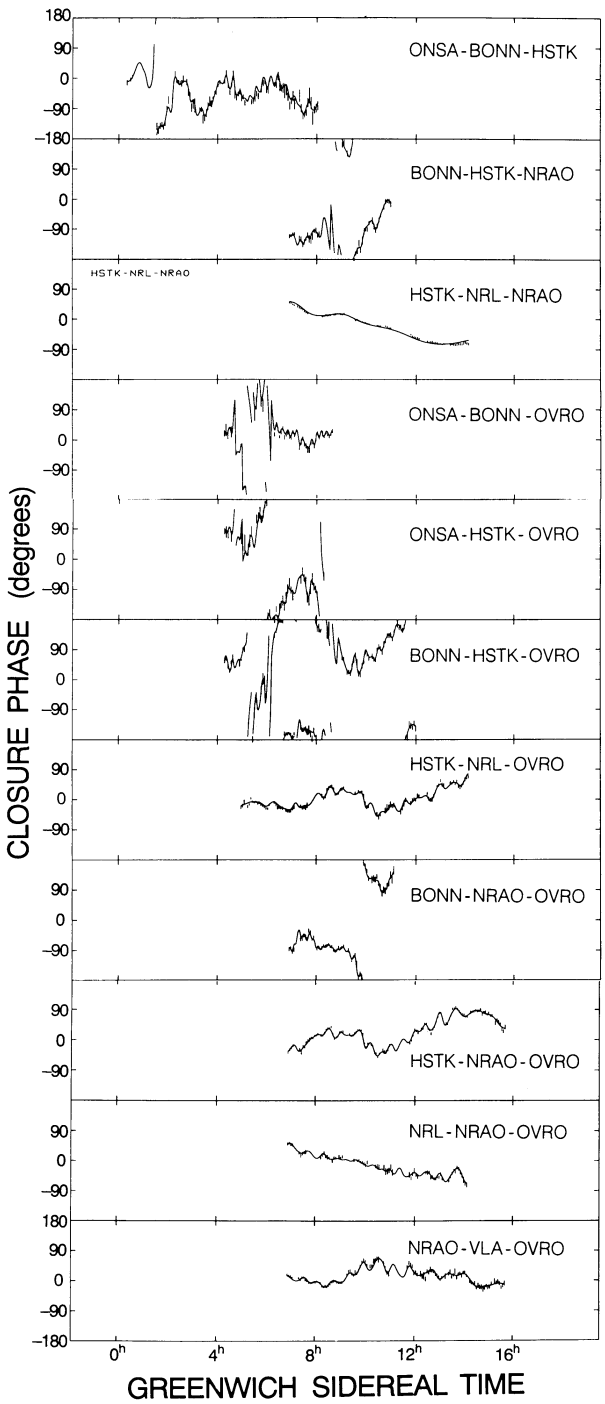

FIG. 5b

FIG. 5.—Fit of the final hybrid map for the first epoch, shown in Fig. 4(*a*), to the self-calibrated visibility data

FIG. 6.—Gray-scale image of the hybrid map of the first epoch—also shown as a contour plot in Fig. 4*a*—clearly indicating the two ridges of emission and the apparent shift between them. This gray-scale image makes it easy to envisage a winding helical structure of constant pitch angle in which the bright portions indicate those regions where the helix is tangential to the line of sight.

better than modeling. A gray-scale image of this map is shown in Figure 6.

We are confident that the structures we have derived from modeling and mapping are correct and that the details of these models and maps can be trusted. We have therefore succeeded in one of the chief aims of this reanalysis—namely—to determine the morphology of the northern and southern components to the limit permitted by the resolution and sensitivity of the observations.

In Table 1 we list the parameters of the Gaussian components of the first epoch model together with the physical properties derived for each component by the usual arguments. In Table 2 we list the model parameters for the second and third epochs.

3. DETAILED COMPARISONS OF THE OBSERVED SMALL-SCALE STRUCTURE FROM 1985 FEBRUARY TO 1986 FEBRUARY

3.1. *The Northern Component*

The three models of the northern component are shown in Figures 3*a*–3*c*. There is a strong similarity between these three models. The five components, marked "A," "B," "C," "D," and "E" appear in almost the same positions in all three models, but with different flux densities. We are confident that this is not merely due to the fact that we used the model from epoch 1 as the starting point for epochs 2 and 3. If this model had not been basically correct, it is most unlikely that it could have been adjusted to fit the very different visibility data from epochs 2 and 3 merely by changing the flux densities of the components. We are, therefore, convinced of the reality of these five components and of the fact that they did not move appreciably over the 1 yr period spanned by these observations. As can be seen in Tables 1 and 2, components "A," "B," "C," and "E" moved by $\lesssim 0.05$ milliarcsec (5×10^{16} cm) and component "D" moved by ~ 0.1 milliarcsec over the period of 1 yr spanned by the observations.

Thus the structure of the northern component revealed by the 22 GHz observations appears to have been fairly stable over the period 1985 February–1986 February, although the relative flux densities and shapes of the components did change appreciably.

3.2. *The Extended Southern Emission and Knot K*

The structure of NGC 1275 changes significantly at about 1.5 mas (~ 0.5 pc) from the northeastern extreme. At this point: (1) the surface brightness drops by over an order of magnitude; (2) the general orientation changes from $\sim -150°$ to $\sim -180°$; and (3) the structure broadens considerably, filling a cone of opening angle $\sim 12°$, and forming a diffuse component which extends down to 11 mas from the core in p.a. 180°.

All of these features are seen in the 1985 February gray-scale image (Fig. 6) and the overall appearance of the southern extended component, is shown most clearly here. This figure, the models, and the corresponding maps reveal that the 10 milliarcsec southern "jet" actually consists of two ridges which might define the sides of a cone of opening angle $\sim 12°$. Note that from 7 to 11 milliarcsec from the compact northern feature the limb-brightened edges of the structure appear to be approximately parallel, so that more observations are needed to establish whether or not this is indeed emission from a cone-shaped feature. For the remainder of this discussion we assume that it *is* a cone.

These images also show that the knot first detected by Readhead et al. (1983a) and studied by Marr et al. (1989) is embedded in the southernmost tip of the eastern ridge. The two ridges mimic each other to a remarkable degree—they are about the same length and they brighten and dim in the same way—and four brightness peaks are seen in each ridge: H, I, J, and K in the eastern ridge and L, M, N, and O in the western ridge. There were also hints of this double ridge structure in the 22 GHz observations made in 1981 (Readhead et al. 1983) and in our earlier analysis of the present observations (Marr et al. 1989), but the lower dynamic range of those maps left some doubt about the reality of the effect. We see from the present maps, especially that of 1985 February, that there can no longer be any doubt about this structure. A very interesting feature of these ridges is the shift between the bright knots in the two ridges. The profiles measured along the lines marked X1, X2, and X3 are shown in Figure 7*a*–7*c*, respectively. In Figure 8*a* we show the profile along X1 together with that along X2, which has been shifted along the line X2 toward the north by 1.5 milliarcsec, and in Figure 8*b* we show the profile along X1 together with that along X3, which has been shifted along the line X3 toward the north by 1.5 milliarcsec. The correlation is striking, suggesting a constant shift, or delay, between features on the eastern side of the cone relative to the western side. Note that such a shift would also make the peak

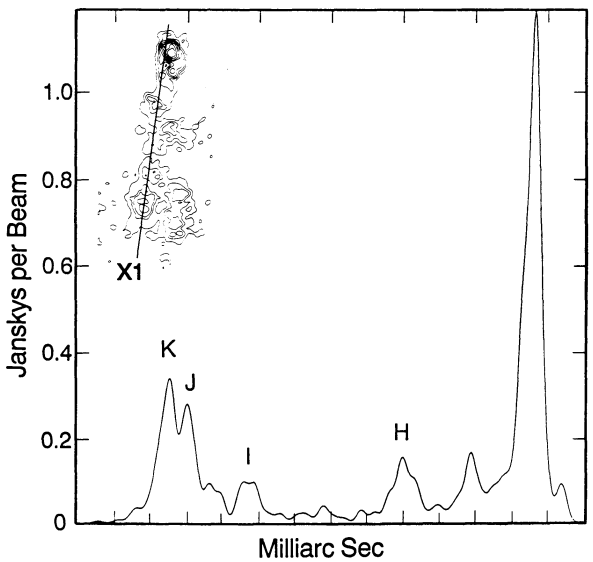

FIG. 7*a*

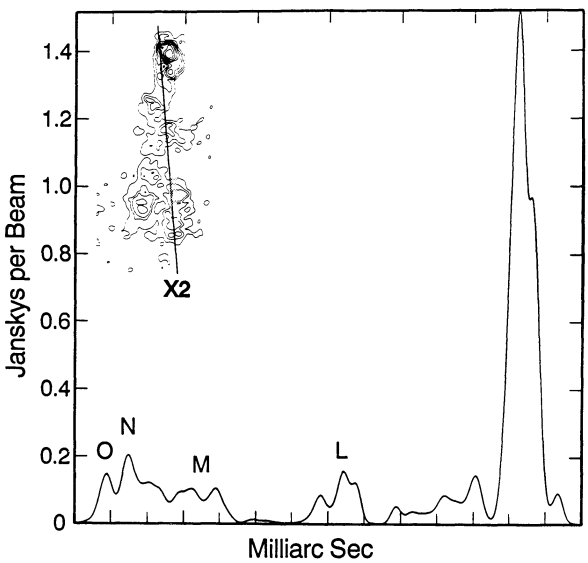

FIG. 7*b*

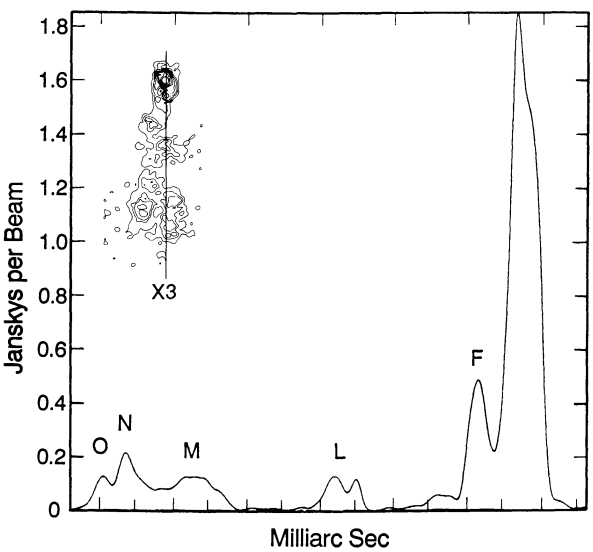

FIG. 7*c*

FIG. 7.—Profiles of the surface brightness along the lines indicated on the inset contour plots. (*a*) Profile through the northeastern extreme of the structure along the eastern edge of the conical jet—along X1. (*b*) Profile through the northeastern extreme of the structure along the western edge of the conical jet—along X2. (*c*) Profile along the western edge of the conical jet—along X3. The peaks of surface brightness, designated H, I, J, and K along X1 are spaced at the same intervals as the peaks of surface brightness, designated L, M, N, and O along X2 and X3

F on X3 coincide with peak A on X1, so that there are five features which are brought into coincidence by this constant shift. The position angle of $-130° \rightarrow -150°$ seen in the northern compact component is similar to that which connects adjacent bright peaks on X1 and X3. The structure looks very like a helical structure in which the bright knots are due to a helical filamentary structure on the surface of the conical jet. On this interpretation the bright regions (H, I, J, K and L, M, N, O) at the edges of the jet cone correspond to points at which the line of sight is running tangential to the filament. The windings of the helix would be approximately equally spaced if there were another turn between the upper turn (peaks H and L) and the lower two turns (peaks I and M and peaks J + K and N + O). There *is* a faint hint of another such turn on the eastern ridge between peaks H and I—just to the southeast of peak L, so this interpretation seems very plausible. Krichbaum et al. (1992) also interpret their 43 GHz results in terms of possible helical structure. Although not absolutely conclusive, the present results provide the strongest evidence yet for such a helical structure. It is unlikely that such a correlation between *five* peaks, as seen in Figure 8(*b*) is a chance occurrence, and we believe that this constant shift in brightness peaks between the eastern and western sides of the jet is not simply due to a random distribution of bright patches, but is telling us something of physical importance about the nature of the jet. Hardee & Clarke (1992) have carried out three-dimensional computer simulations of jets, taking into account the magnetic field, and found that helical patterns are often produced by the Kelvin-Helmholtz instability. If this helical structure in NGC

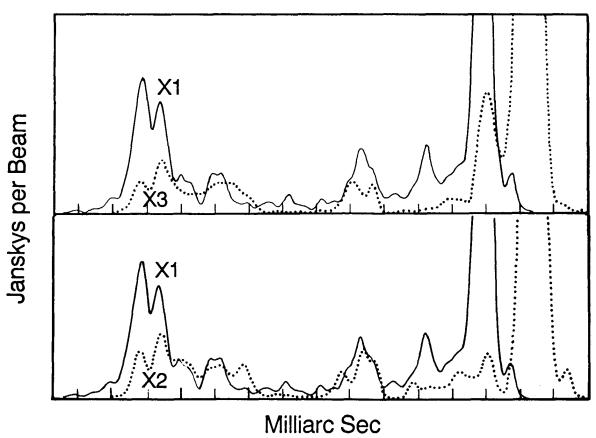

FIG. 8.—Correlation between the brightness levels along the eastern and western profiles. A constant shift of ~1.5 milliarcsec of the eastern relative to the western cuts would bring the high surface brightness regions into coincidence. (*a*) Comparison between the profiles along X1 and X2 after relative shift of 1.5 milliarcsec. (*b*) Comparison between the profiles along X1 and X3 after relative shift of 1.5 milliarcsec.

1275 is confirmed by better observations then changes in this structure with time could provide important clues to the magnetohydrodynamics of the jet and possibly to the central engine itself.

Knot K, at the southern end of the eastern ridge, is well known, and its kinematics have been discussed by Marr et al. (1989). Our model fitting allowed us to follow the path of this component with great accuracy. Taken at face value, the results given in Table 1 for the three epochs analyzed here indicate an acceleration of knot K from 0.47c between 1985.17 and 1985.83 to 0.96c between 1985.83 and 1986.17, but this is more likely due to measurement errors than a real acceleration. If we fit a constant velocity for this period, consistent with the errors, we find $v_{app}/c = 0.63 \pm 0.15$, in agreement with our earlier measurements (Marr et al. 1989, 1990).

4. COMPARISON WITH HIGHER FREQUENCY RADIO OBSERVATIONS

The main differences between the present study and those undertaken by Bartel et al. (1988) and by Krichbaum and his collaborators in an extensive series of observations (1990, 1992) lie in the details in the northern and southern components and in the dynamic range of the maps. There are striking similarities between our maps and models of NGC 1275 and those derived from 43 GHz observations, which show clearly that the northern component consists of a number of very compact components extending along a line at position angle $-135° \rightarrow -150°$, and a component, or ridge extending to the north. These features are clearly seen in all three of our models. In the present analysis the detailed morphology of the northern structure is better defined—because we have more data, it is of higher quality due to the higher aperture efficiencies at 22 GHz, and the calibration is more accurate—and can be used to determine the relative motions, if any, of these persistent features over the 1 yr period spanned by the observations.

Observations of NGC 1275 at 90 GHz have been made at a number of epochs (Readhead et al. 1983b; Backer 1987; Wright et al. 1988). At 90 GHz only the most compact features are visible due to a combination of the steep spectra of many of the components and the sensitivity limitations of the available millimeter telescopes. The observations are most readily interpreted in terms of a compact ($\lesssim$0.1 milliarcsec) component with a 0.5–1 milliarcsec extension in position angle 135°–155°, consistent with the structures observed at 43 and at 22 GHz.

5. PHYSICAL PROPERTIES

One of the most important physical properties of the nuclear emission regions in active galaxies is the mass of the central engine. There are, as yet, no direct and convincing methods for estimating this mass. Plausible limits can be obtained by the usual arguments—an upper limit to the mass of the central engine can be estimated assuming that the broad line clouds are gravitationally bound to the central engine. The full width at zero intensity of the Hα line is $\sim$10,000 km s^{-1}, which, at a radius of $\sim 10^{17}$ cm often used as a crude estimate of the size of the broad emission-line region, yields a mass of $\sim 10^9\ M_\odot$.

A lower limit to the central mass is provided by the Eddington limit given by

$$M_E = 8 \times 10^3 \left(\frac{L_{bol}}{10^{42}\ \mathrm{ergs^3\ s^{-1}}} \right) M_\odot ,$$

which yields $1.2 \times 10^6\ M_\odot$ for the value of L_{bol} given below.

The study of the physics of most compact radio emission regions in active galactic nuclei is complicated by strong relativistic effects. In the case of NGC 1275 any apparent motion is subluminal (Romney et al. 1982, 1984; Marr et al. 1989, 1990) as we have seen is the case for knot K. Furthermore Readhead et al. (1983a) showed that the inverse Compton emission predicted from the radio emission regions is very close to that actually observed in the compact X-ray source. There is thus no evidence of relativistic beaming. We therefore assume that relativistic effects are not important in the emission observed from this object.

We have carried out the standard calculations of the equipartition magnetic fields, synchrotron lifetimes of the radiating electrons, etc., assuming that the radiation from all of the observed components is isotropic. We assumed further that the upper and lower cutoffs in the spectrum are at 10 MHz and 100 GHz, respectively, and that all components have optically thin spectral index $\alpha = -0.75$, where $S \propto \nu^\alpha$. The results of these calculations are given in Table 1 for the model derived from the first epoch observations (1985 February). It can be seen that the brightness temperatures of the observed components range from 4×10^9–1.5×10^{11} K, the equipartition magnetic fields range from 0.1 to 0.7 G and the minimum energies range from 2×10^{50}–3×10^{52} ergs. The smallest features are 1.7×10^{17} cm across.

Begelman, Blandford, & Rees (1984) showed that if an active galactic nucleus is powered by steady radial accretion onto a black hole then the minimum mean optical depth is

$$\tau_{THOMSON} \geq \left(\frac{\dot{M}}{\dot{M}_E} \right) \left(\frac{r}{r_g} \right)^{-1/2} \left(\frac{v_{free\ fall}}{v_{in\ fall}} \right) ,$$

where r_g is the gravitational radius of the black hole (GM/c^2), so that for $r \sim 0.4$ mas (0.13 pc), $M = 10^8\ M_\odot$, and the other bracketed factors of order unity we have $\tau_{THOMSON} \gtrsim 0.1$ and $n_e \gtrsim 4 \times 10^5$ cm^{-3}. If these conditions prevailed around the central engine of NGC 1275 we would expect to see some evidence of thermal plasma due to Thomson scattering (see, e.g., Readhead, Cohen, & Blandford 1978), and possibly also due to induced Compton scattering (Coppi, Blandford, & Rees 1992) or stimulated Raman scattering.

Electromagnetic wave propagation through a plasma can scatter off both electrons and plasma waves (see, e.g., Thompson et al. 1993). The electron scattering is called Compton scattering, and in cases where the brightness temperature is sufficiently high one has induced Compton scattering in which the Compton shift in frequency associated with the electron recoil is taken into account. The effect is strongly frequency dependent and can therefore cause significant distortions of the emitted spectrum. Collective plasma wave scattering occurs through the creation and destruction of Langmuir plasmons (the quanta of Langmuir waves) by radio wave photons and is called Raman scattering (Thompson et al. 1993). One must consider two cases: "strong" Raman scattering and "weak" Raman scattering. In strong scattering the plasmons grow at such a rapid rate that there does not exist a competitive damping process, so the growth happens without restriction. In weak scattering, which is more relevant for active galactic nuclei, the spatial growth of instabilities occurs at a rate which is constrained by decay through damping. There is a specific length for damping and hence weak scattering has a length scale. Unlike the case of induced Compton scattering, there is no strong frequency dependence in Raman scattering. The possibilities of induced Compton scattering and Raman scattering in NGC 1275 are considered below.

Coppi et al. (1992) show that, assuming a situation is which the synchrotron source is embedded in thermal gas, the optical depth due to induced Compton scattering constrains the electron density out to a distance r from the source to be

$$n_e \lesssim 7000 T_{12}^{-1} r_{\rm pc}^{-1} \ {\rm cm}^{-3} .$$

In NGC 1275 the most stringent upper limit on n_e is provided by component B, which has $T_{12} = 0.15$. If we consider the region in the "jet" within 0.5 mas (0.17 pc) of component B we deduce for this region that $N_e \lesssim 3 \times 10^5$ cm^{-3}. Following the argument of Coppi et al., this places a constraint on the pressure of $p < 5 \times 10^{-5} M_{\rm h8} T_{12}^{-1} r_{\rm pc}^{-2}$ dyne cm^{-2} for the component of interest here. Thus for a $10^8 \ M_\odot$ black hole, $T = 1.5 \times 10^{11}$ K and $r = 0.17$ pc, we have $p < 10^{-2}$ dyne cm^{-2}. In Table 1 we have listed the minimum pressures in the various radio emission regions. Since these are minimum pressures we see that the northern compact component cannot be confined by thermal gas pressure in the surrounding medium, but must either be free or magnetically confined, unless the mass of the central engine is significantly greater than $10^8 \ M_\odot$. Furthermore any significant amount of induced Compton scattering would effectively quench the radio source. Therefore the effect of thermal plasma and any induced Compton scattering must be small. This strongly suggests that the jet region and the accreting region are separate (Coppi et al. 1992), a situation which could arise, for example, in the case where the radio emission comes from a jet along the spin axis of the central engine, and the optical emission regions are confined to the regions in and around an equatorial accretion disk. There might, however, be weak induced Compton scattering which would give raise to faint radio structure. What is clearly needed are much higher dynamic range maps which would enable us to detect faint features around the compact components seen here and which might provide direct evidence of induced Compton scattering. High-frequency polarization observations with the VLBA will be particularly important in this regard.

We next consider the possible effects of Raman scattering (Thompson et al. 1993) in the northern compact feature of NGC 1275. R. Blandford (1992, private communication) has estimated that strong Raman scattering requires

$$T_b \geq 10^{16} p_{-3}^{-1/2} \nu_9 ,$$

so that for p $\geq 10^{-2}$ dyne cm^{-2}, such as we have in components A–E, at 22 GHz, strong Raman scattering requires brightness temperatures in excess of 7×10^{12} K, considerably greater than those found in these components. Blandford (1992, private communication) has also estimated that the condition for weak stimulated Raman scattering is

$$T_b \geq 10^{12} T_6^{-1/4} \tau_{\rm THOMSON}^{-1/2} \left(\frac{\Delta\Omega}{2\pi} \right)^{-1} ,$$

so that in a "standard" intercloud medium with $\tau_{\rm THOMSON} \sim 0.1$ and $T_6 \sim 10^2$, the requirement for weak Raman scattering is that the brightness temperature should exceed 10^{12} K. It appears, therefore, that we may ignore the effects of Raman scattering in NGC 1275 but not the effects of induced Compton scattering.

The thermal plasma might be seen illuminated by the radio emission regions through either induced emission, or, possibly, backscattered radiation, and might be faintly visible at a level about two orders of magnitude fainter than the bright emission regions (Coppi et al. 1992). Such emission might therefore be seen in NGC 1275 in very high dynamic range radio images. Clearly, a major objective of future VLBI observations of this object should be to search for evidence of this thermal plasma, since this might delineate the accretion disk itself and greatly aid the interpretation of the extremely complex structure we have found in this object.

6. DISCUSSION

The morphology of 3C 84, as it emerges from our maps, is complicated. The most dramatic feature in the images presented here is the abrupt change in structure observed 1.5 milliarcsec (0.5 pc) south of the northernmost feature. The other main morphological features to be accounted for are: (1) the edge-brightened cone of emission; (2) the correlation between the bright regions along the two edges of the cone, together with the relative shift of 1.5 milliarcsec (0.5 pc) of corresponding bright regions along the edges; (3) the compact structures observed in the northern region; and (4) the subluminal knot K.

6.1. *The Change in Morphology at 0.5 pc*

The abrupt change in the morphology of the nuclear emission region at 0.5 pc in NGC 1275 is very likely due to a substantial change in the physical conditions which dominate the dynamics of the outflowing material at this distance. The structure we see here is similar to the well-known gaps often seen between the cores and the jets in Fanaroff-Riley Type I objects. We consider four possible causes in the following sections: (1) that this is a *de Laval* nozzle (Blandford & Rees 1974) in which the jet is confined by thermal pressure such that the material is subsonic at distances smaller than 0.5 pc from the northern extreme of the structure and supersonic at greater distances; (2) that the outflowing material encounters a preexisting standing shock at a distance of 0.5 pc from the central engine, and this causes a serious disruption of the jet material as has been suggested on much larger scales in some other objects by Norman, Burns, & Sulkanen (1988, hereafter NBS); (3) that the nuclear jet collides with a much denser medium at this point; and (4) that the distance of 0.5 pc is the distance from the central engine at which there is a transition from a region in which the gravitational potential is dominated by the central engine to one where the potential due to the material in the inner regions of the galaxy itself preponderates over that due to the central engine.

6.1.1. *de Laval Nozzle*

The possibility that a de Laval nozzle at 0.5 pc is responsible for the structure in this region seems unlikely. We have seen that typical minimum pressures in the northern components "A"–"E" are in the range $1.5–4 \times 10^{-2}$ dyne cm^{-2}—substantially greater than the upper limit placed on the pressure by the absence of significant induced Compton scattering, unless the mass of the central engine is greater than $\sim 10^9 \ M_\odot$, and there is no evidence of significant Thomson scattering.

6.1.2. *Transition through a Standing Shock*

If the jet starts well within the northern component, and if the dominant position angle within the first few tenths of a parsec indicates the initial jet direction, then we may have a radio jet emitted in p.a. $\sim -150°$ which is disrupted at ~ 0.5 pc. Almost any significant discontinuity in the ambient medium could disrupt the jet. For example, NBS consider dis-

ruption in less powerful objects by a standing shock in the interstellar medium, which might be caused by a wind due to the active nucleus and give rise to conical structures similar to that observed in NGC 1275. NBS considered the disruption of a jet when it encounters a shock in the external medium perpendicular to the flow direction along the jet and showed that to disrupt the jet we require $M_{\rm jet}/M_{\rm ext} < 1$ in the region before the shock front, where M is the Mach number. The opening angle of the jet is 12°, giving a cone angle ψ, as defined by NBS, of 6°, which implies that $M_{\rm jet}/M_{\rm ext} \sim 0.15$ provided that $M_{\rm jet} \gg 1$.

On this model the jet would be supersonic before traversing the shock and subsonic thereafter. The cone angle, ψ, is comparable to that subtended by the kiloparsec-scale double structure observed by Pedlar et al. (1986), so that the material would have to continue to flow outward in this cone to scales $\sim 10^{22}$ cm. However, we feel that there are some difficulties with this model, which also apply to the following scenario, and which we therefore discuss below.

6.1.3. *Collision with Dense Medium*

A jet could be disrupted by colliding with a much denser neutral region in the external medium. The existence of molecular clouds and of a dense medium on scales of parsecs is gaining observational support on the basis of optical spectropolarimetry of active galaxies (see Miller 1989 and references therein). A possible theoretical scenario for the "intermediate" zone is given by Krolik (1989), who suggests that this intermediate zone is an optically and geometrically thick torus, formed mainly by dust and gas. The material in this torus would be clumpy, with very large random velocities. In the Krolik model the thickness of the torus (i.e., the solid angle covered by the torus) is a variable parameter, and it can be anything from a thin layer to a spherical shell. In the present case it would have to be a spherical shell in order to disrupt the jets directed along the spin axis of the central engine.

It is possible that the jet disrupts and flares out when it crosses the border of the intermediate zone. CO observations by Mirabel et al. (1989), indicate that an estimated mass of $\sim 3 \times 10^9\ M_\odot$ of molecular gas is present in the center of NGC 1275. In this scenario the jet would be disrupted when entering the intermediate zone, where it would entrain material and expand in order to reach pressure equilibrium with the external medium.

Problems with these models.—Although the two mechanisms discussed in §§ 6.1.2 and 6.1.3 could disrupt the jet, we think it unlikely that either is responsible for the abrupt change in structure at 0.5 pc. The helical structure seen in the material flowing south is the strongest argument against serious disruption of the jet. Furthermore the VLA map by Pedlar et al. (1986) shows quite clearly the existence of two bright hot spots along the southern jet. For these reasons this does not look like a jet which has entrained a lot of material, or which has been disrupted and is dominated by turbulent motions, as suggested in the case of 1231+674 by NBS. It is possible that there has been some recollimation (e.g., by a de Laval nozzle) on a scale 10^{19}–10^{20} cm, and that the jet has therefore been reformed, but neither the structure on the scale 10^{18}–10^{19} cm nor the large-scale structure readily support the notion of a highly disrupted jet.

6.1.4. *Transition from Central-Engine to Galaxy-Dominated Potential*

If we postulate that the transition at 0.5 pc in radio structure indicates the physical transition from the region dominated by the potential of the central engine to the region where the dynamics are dominated by the galactic potential and assume that the virial velocities at this distance from the central engine are ~ 300 km s^{-1}, the corresponding mass of the central engine would be $4 \times 10^7\ M_\odot$, consistent with the upper and lower limits derived in the previous section. How this transition would be manifest in the observations is unclear, and we advance no specific model to account for the structural change. What is clear, however, is that the region in which this important transition occurs lies within the range of physical scales that we have observed here (i.e., between 10^{17} cm and 10^{19} cm), unless the mass of the central engine is greater than $5 \times 10^8\ M_\odot$. In this regard the factor of 30 better linear resolution that we have on this object, compared with other objects of similar luminosity, is crucial, since it places this critical transition region in the accessible range of angular scales, whereas we believe that in general in powerful extragalactic radio sources the region dominated by the central engine is smaller than the highest resolution afforded by ground-based VLBI. At the outer limit of the broad line region (~ 0.05 pc) a central mass of $4 \times 10^7\ M_\odot$ would bind objects with velocities less than 1000 km s^{-1}. We note that the extreme broad line clouds are moving with speeds 10 times higher, that is, 10^4 km s^{-1} and would therefore be unbound.

6.2. *The Cone of Emission*

We believe that the cone or double ridge morphology of the extended emission region will be important to understanding the physics of this object, but the quality of the present observations is not good enough to be certain of the details of this region. As discussed above, the features that we see could well be due to filamentary structure following a helical path along the surface of the cone. Such a structure has been observed in the jet in M87 (Biretta, Owen, & Cornwell 1989). In the case of NGC 1275, there is much more rapid structural variation than in M87, so that this might prove a more fruitful object for the study of changes in these filaments with time. If these filaments are confirmed by subsequent observations, they should provide an important testing ground for the theory of relativistic magnetohydrodynamic flows and shocks. It should be a relatively simple matter with the VLB Array to monitor changes in the positions of the bright features on the two limbs of the cone, and it will be interesting to see whether these all move southwards at a constant velocity. It will also be interesting to determine whether the offset in the separation from the core of the bright features in the eastern and western limbs of the cone is constant or varying with time.

7. CONCLUSIONS

The radio structure of the central regions of NGC 1275 is far more complex than is usually observed in active galactic nuclei. We may here be seeing, for the first time, the structure of a region under the influence of the gravitational potential of the central engine. It is clearly of great importance to determine the longevity of the features which have been observed, and to determine whether these are random structures in a highly shocked environment, or whether they exhibit features which can be traced directly to the central engine itself—that is, the putative accretion disk and black hole. For example, the resolution afforded by these observations would be sufficient to resolve a supermassive binary black hole, if it existed, in the nucleus of this galaxy, unless it were very close to coalescing. Careful monitoring of this region promises to be a fruitful line

of attack on this interesting object. At larger distances from the nucleus, the suggestive cone-shaped emission region reveals aspects of a relativistic flow which vary on time scales of months. Limb-brightened hotspots on this cone might be due to a helical structure on the surface of the cone, similar to, but on a smaller scale than, such structures observed in other objects. Over the next decade we anticipate a dramatic improvement in the quality of images of this object at 22 and 43 GHz, with the advent of the VLB Array and orbiting VLBI telescopes. This object will therefore provide an important opportunity for testing theories of relativistic jets. Significant structural variations over time scales of a few months should reveal many details of the activity in active galactic nuclei which are inaccessible in more distant objects of comparable power.

We thank Roger Blandford for many useful and critical comments and for providing us with details of induced Compton scattering and stimulated Raman scattering prior to publication. We also thank Sterl Phinney for useful discussions and the staffs of the observatories in the global VLBI network for their care and attention in making these observations. We thank T. J. Pearson for many useful changes to the Caltech VLBI software package, without which this work would not have been possible. T. Venturi gratefully acknowledges the receipt of a CNR/NATO fellowship, N. 203.02.19, during the period that this work was carried out. The work at Caltech was supported by National Science Foundation grants AST 85-09822, AST 88-14554, and AST 91-17100; and the work at the University of California, Berkeley was partially supported by National Science Foundation grant AST 84-16177.

REFERENCES

Backer, D. C. 1987, in Superluminal Radio Sources, ed. J. A. Zensus & T. J. Pearson (Cambridge: Cambridge Univ. Press), 76
Bartel, N., et al. 1988, Nature, 334, 131
Begelman, M. C., Blandford, R. D., & Rees, M. J. 1984, Rev. Mod. Phys., 56, 255
Biretta, J. A., & Owen, F. N. 1990, in Parsec-Scale Radio Jets, ed. J. A. Zensus & T. J. Pearson (Cambridge: Cambridge Univ. Press), 125
Biretta, J. A., Owen, F. N., & Cornwell, T. J. 1989, AJ, 342, 128
Blandford, R. D., & Rees, M. J. 1974, MNRAS, 169, 395
Branduardi-Raymont, G., et al. 1981, 248, 55
Coppi, P., Blandford, R. D., & Rees, M. J. 1992, MNRAS, in press
Fabian, A. C., Hu, E. M. Cowie, L. L., & Grindlay, J. 1981, ApJ, 248, 47
Grindlay, J., Branduardi, G., & Fabian, A. 1980, in Highlights Astron., 5, 741
Hardee, P. E., & Clarke, D. A. 1992, ApJ, 400, L9
Impey, C. D., & Neugebauer, G. 1988, AJ, 95, 307
Kent, S. M., & Sargent, W. L. W. 1979, ApJ, 230, 667
Krichbaum, T. P. 1990, in Parsec-Scale Radio Jets, ed. J. A. Zensus & T. J. Pearson (Cambridge: Cambridge Univ. Press), 83
Krichbaum, T. P., et al. 1992, A&A, in press
Krolik, J. H. 1989, in IAU Symp. 134, Active Galactic Nuclei, ed. D. E. Osterbrock & J. S. Miller (Dordrecht: Reidel), 285
Lyuti, V. M. 1977, AZh., 54, 1153
Marr, J. M., Backer, D. C., & Wright, M. C. H. 1990, in Parsec-Scale Radio Jets, ed. J. A. Zensus & T. J. Pearson (Cambridge: Cambridge Univ. Press), 78
Marr, J. M., Backer, D. C., Wright, M. C. H., Readhead, A. C. S., & Moore, R. 1989, ApJ, 337, 671
Miller, J. S. 1989, in Active Galactic Nuclei (Berlin: Springer), 112
Mirabel, I. F., Sanders, D. B., & Kazes, I. 1989, ApJ, 340, L9
Norman, M. L., Burns, J. O., & Sulkanen, M. E. 1988, Nature, 335, 146 (NBS)
Pearson, T. J., & Readhead, A. C. S. 1984, ARA&A, 22, 97
———. 1988, ApJ, 328, 114
Pearson, T. J. 1991, BAAS, 23, 991
Pedlar, A., Ghataure, H. S., Davies, R. D., Harrison, B. A., Perley, R., Crane, P. C., & Unger, S. W. 1990, MNRAS, 246, 477
Pedlar, A., Perley, R., Crane, P., Harrison, B., & Davies, R. D. 1986, in Radio Continuum Processes in Clusters of Galaxies, ed. C. P. O'Dea & J. M. Uson (NRAO: Greenbank), 135
Readhead, A. C. S. 1990, in Modern Technology and its Influence on Astronomy, ed. J. V. Wall & A. Boksenberg (Cambridge: Cambridge Univ. Press), 71
Readhead, A. C. S., Cohen, M. H., & Blandford, R. D. 1978, Nature, 272, 131
Readhead, A. C. S., Hough, D. H., Ewing, M. S., Walker, R. C., & Romney, J. D. 1983a, ApJ, 265, 107
Readhead, A. C. S., et al. 1983b, Nature, 303, 504
Readhead, A. C. S., Venturi, T., Marr, J. M., & Backer, D. C. 1990, in Parsec-Scale Radio Jets, ed. J. A. Zensus & T. J. Pearson (Cambridge: Cambridge Univ Press), 71
Readhead, A. C. S. Walker, R. C., Pearson, T. J., & Cohen, M. H. 1980, Nature, 285, 173
Readhead, A. C. S., & Wilkinson, P. N. 1978, ApJ, 223, 75
Romney, J. D., Alef, W., Pauliny-Toth, I. I. K., & Preuss, E. 1984, in IAU Symp. 110, VLBI and Compact Radio Sources, ed. R. Fanti, K. I. Kellermann, & G. Setti (Dordrecht: Reidel), 137
Romney, J. D., Alef, W., Pauliny-Toth, I. I. K., Preuss, E., & Kellermann, I. I. K. 1982, in IAU Symp. 97, Extragalactic Radio Sources, ed. D. S. Heeschen & C. M. Wade (Dordrecht: Reidel), 291
Rubin, V. C., Ford, W. K., Peterson, C. J., & Oort, J. H. 1977, AJ, 211, 693
Thompson, C., Blandford, R. D., Evans, C. R., & Phinney, E. S. 1993, ApJ, submitted
Unwin, S. C., Mutel, R. L., Phillips, R. B., & Linfield, R. P., 1982, ApJ, 256, 83
Wilkinson, P. N., Readhead, A. C. S., Purcell, G. H., & Anderson, B. 1977, Nature, 269, 764
Wright, M. C. H., et al. 1988, ApJ, 329, L61
Zensus, J. A., Hough, D. H., & Porcas, R. W. 1987, Nature, 325, 36